Supporting Information

Two New Coordination Polymers, a Trinuclear Metal Complex and Their Interconversion depending on Solvent

Shiori Koike,[1] Takeshi Hirakawa,[1] Katsunori Yamanishi,[2] and Mitsuru Kondo[1,3]*

[1] Department of Chemistry, Faculty of Science, Shizuoka University, 836 Ohya, Suruga-ku, Shizuoka, 422-8529 Japan

2 Graduate School of Science and Technology, Shizuoka University, 836 Ohya, Suruga-ku, Shizuoka 422-8529 Japan.

[3] Green Chemistry Research Division, Research Institute of Green Science Technology, Shizuoka University, 836 Ohya, Suruga-ku, Shizuoka 422-8529, Japan

E-mail: scmkond@ipc.shizuoka.ac.jp

Table of Contents

1. Instrumentation and Materials.

All solvents and reagents were of the commercial reagent grade and used without further purification. The water was used ion-exchanged water. IR spectra were recorded on Shimadzu IR Affinity-1 using KBr pellets. UV-vis-NIR reflection spectra were recorded on a Jasco V-570. Elemental analyses were measured using Euro Vector EA 3000. Crystallographic data were collected by Rigaku CCD mercury system using graphite-monochromated Mo Kα radiation (λ = 0.71070 Å) at 20 °C or -100 °C. X-ray Powder Diffraction Patterns were observed using Rigaku MiniFlex 600 diffractometer equipped with graphite monochromated Cu Kα radiation (λ = 1.54073 Å). The ligand bitb was synthesized by according to the previously reported method[1].

1) a) T. Hirakawa, M. Yamaguchi, N. Ito, M. Kondo, M. Miyazawa, N. Nishina, S. Yasue, K. Maeda, F. Uchida, *Chem. Lett.* **2009**, *38*, 290-291. b) M. Yamaguchi, T. Hirakawa, N. Ito, N. Nishina, M. Kondo, H. Aoki, E. Okuda, L. Zhang, *Chem. Let.*, **2010**, *39*, 1192-1193. c) T. Inoue, K. Yamanishi, M. Kondo, *Inorg. Chem.* **2013**, *52*, 4765-4767.

2. Experimental Section

Synthesis of {[Cu(bitb)$_2$(NCS)]NCS·2MeOH·H$_2$O}$_n$ (1)

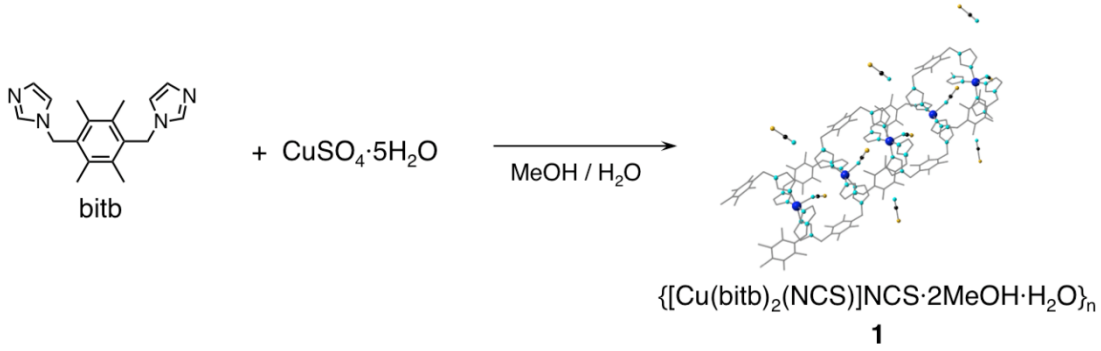

Scheme S1.

A methanol solution (30 mL) of bitb (0.141 g, 0.48 mmol), a MeOH / H_2O (1:1, v/v) mixed solution (30 mL) of NaSCN (0.039 g, 0.48 mmol), and an aqueous solution (30 mL) of $CuSO_4·5H_2O$ (0.060 g, 0.24 mmol) were mixed and stirred for a few days. The obtained blue powder was collected by filtration and dried under air. (0.097 g, 0.11 mmol, 47.5 % yield). Anal. Calcd. for $C_{40}H_{54}CuN_{10}O_3S_2$ (850.60): C, 56.48; H, 6.40; N, 16.47. Found: C, 56.55; H, 6.22; N, 16.51. IR (KBr, cm^{-1}): 3449 (m), 3117 (m), 2994 (w), 2945 (w), 2087 (s), 1614 (w), 1520 (m), 1487 (m), 1449 (w), 1437 (w), 1402 (w), 1314 (w), 1294 (w), 1279 (w), 1231 (m), 1109 (s), 1094 (s), 1036 (w), 949 (m), 835 (m), 816 (w), 746 (m), 660 (m), 638 (w), 617 (w).

Single crystals for X-ray structure analysis were obtained as blue needles by diffusion of a methanol solution (10 mL) of bitb (0.024 g, 0.08 mmol) and NaSCN (0.006 g, 0.08 mmol) into an aqueous solution (10 mL) of $CuSO_4·5H_2O$ (0.010 g, 0.04 mmol) for a week (0.011 g, 0.0129 mmol, 32.3 % yield).

Homogeneity of the bulk sample was confirmed by comparison of its X-ray powder diffraction (XRPD) pattern with that of the simulated pattern based on the single crystal data (Figure S6).

Synthesis of {[Cu(bitb)(NCS)$_2$(H$_2$O)]THF}$_n$ (2)

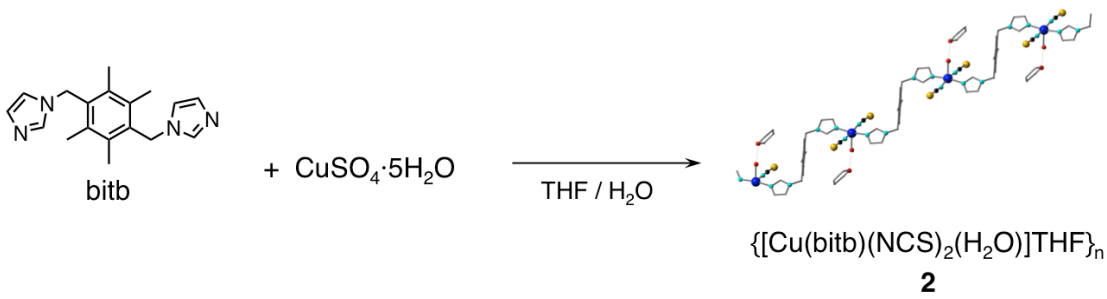

Scheme S2.

A tetrahydrofuran solution (30 mL) of bitb (0.071 g, 0.24 mmol), a THF / H_2O (1:1, v/v) mixed solution (30 mL) of NaSCN (0.039 g, 0.48 mmol), and an aqueous solution (30 mL) of $CuSO_4 \cdot 5H_2O$ (0.060 g, 0.24 mmol) were mixed and stirred for a few days. The obtained light green powder was collected by filtration and dried under air. (0.087 g, 0.15 mmol, 64.2 % yield). Anal. Calcd for $C_{24}H_{32}CuN_6O_2S_2$ (564.22): C, 51.09; H, 5.72; N, 14.89. Found: C, 51.30; H, 5.74; N, 14.41. IR (KBr, cm^{-1}): 3993 (m), 3979 (m), 3566 (w), 3526 (w), 3391 (w), 3150 (w), 3125 (m), 2997 (w), 2909 (w), 2091 (s), 1612 (w), 1531 (m), 1516 (m), 1483 (m), 1447 (w), 1435 (w), 1398 (w), 1383 (w), 1335 (w), 1319 (w), 1285 (w), 1227 (s), 1098 (s), 1036 (w), 1007 (w), 951 (m), 824 (m), 754 (s), 652 (s), 619 (w), 482 (w).

The single crystals for X-ray structure analysis were obtained as green needles by diffusion of a THF solution (10 mL) of bitb (0.012 g, 0.04 mmol) and NaSCN (0.006 g, 0.08 mmol) into an aqueous solution of $CuSO_4 \cdot 5H_2O$ (0.010 g, 0.04 mmol) for a week (0.009 g, 0.016 mmol, 41.2 % yield).

Homogeneity of the bulk sample was confirmed by comparison of its X-ray powder diffraction (XRPD) pattern with that of the simulated pattern based on the single crystal data (Figure S7).

Synthesis of $[Cu_3(bitb)_4(NCS)_6]$ (3)

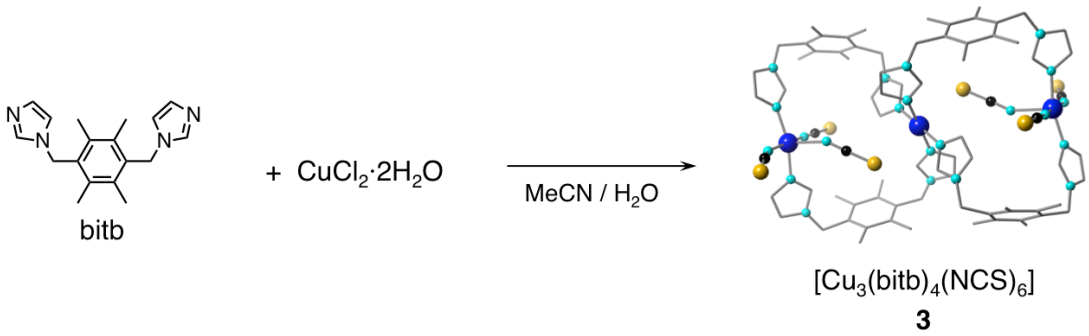

Scheme S3.

An acetonitrile solution (30 mL) of bitb (0.071 g, 0.24 mmol), a MeCN / H_2O (1:1, v/v) mixed solution (30 mL) of NaSCN (0.029 g, 0.36 mmol), and an aqueous solution (30 mL) of $CuCl_2 \cdot 2H_2O$ (0.031 g, 0.18 mmol) were mixed and stirred for a few days. The obtained green powder was collected by filtration and dried under air. (0.063 g, 0.037 mmol, 61.2 % yield).

Anal. Calcd. for $C_{78}H_{88}Cu_3N_{22}S_6$ (1716.70): C, 54.57; H, 5.17; N, 17.95. Found: C, 54.58; H, 5.18; N, 18.01. IR (KBr, cm^{-1}): 3997 (m), 3725 (w), 3524 (w), 3447 (w), 3422 (w), 3115 (m), 2995 (w), 2940 (w), 2911 (m), 2739 (w), 2091 (s), 2085 (s), 1923 (w), 1672 (w), 1612 (w), 1518 (s), 1487 (m), 1449 (m), 1437 (m), 1404 (m), 1389 (m), 1315 (m), 1294 (w), 1271 (w), 231 (s), 1107 (s), 1094 (s), 1076 (m), 1034 (w), 951 (m), 858 (w), 837 (m), 814 (m), 770 (m), 754 (m), 746 (s), 648 (s), 640 (w), 619 (m), 415 (m).

Single crystals for X-ray structure analysis were obtained as green plates by diffusion of an acetonitrile solution of bitb (0.012 g, 0.04 mmol) and NaSCN (0.005 g, 0.06 mmol) into an aqueous solution of $CuCl_2 \cdot 2H_2O$ (0.005 g, 0.03 mmol) for a week (0.009 g, 0.005 mmol, 52.4 % yield).

Homogeneity of the bulk sample was confirmed by comparison of its X-ray powder diffraction (XRPD) pattern with that of the simulated pattern based on the single crystal data (Figure S8).

Structural Conversions among 1, 2 and 3.

Structural changes of each compound by contact with organic solvents were studied by measurements of the XRPD patterns of each bulk sample after immersing in the organic solvents (MeOH, THF, MeCN) for two weeks. The XRPD patterns of the powder sample before and after the immersion in organic solvents were shown in from Figures S9 to S14.

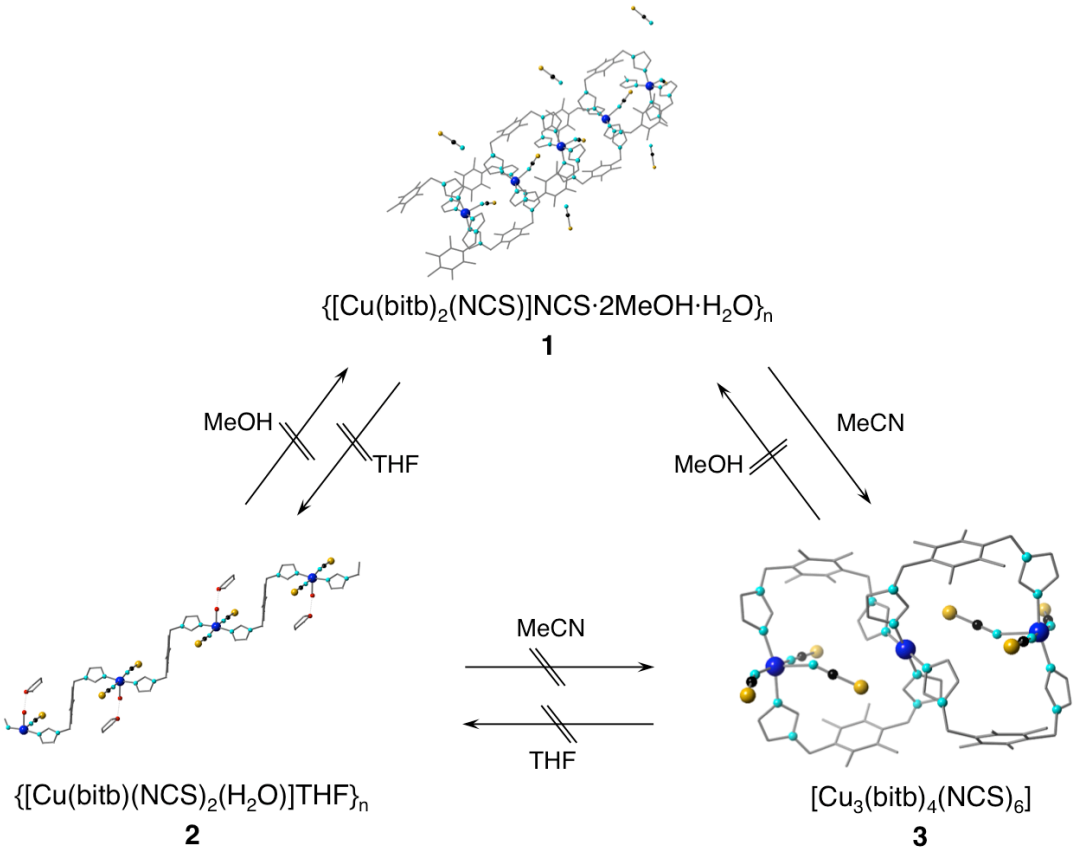

Scheme S4.

3. Crystal Structures

X-ray Diffraction Studies

Single crystal was mounted on a loop for a measurement at 173 K or sealed in a glass capillary with its mother liquid for measurement at 293 K. Data collections were carried out on a Rigaku VariMax (Mo $K\alpha$ radiation, 1.2-kW rotating anode). The summarized data of the X-ray measurements are given in Table S1. For each measurement, eighteen preliminary data frames were measured at 0.5° increments of ω, to assess the crystal quality and preliminary unit cell parameters. The intensity images were also measured at 0.5° intervals of ω. The intensity images were integrated using the CrystalClear program package, and the empirical absorption correction was applied for the data. The structures were solved by direct method, SIR92 program, and refined using the SHELXL-97 program.

Coordination environments and network structures of each compound are shown in Figure S1 and S2 for **1**, S3 and S4 for **2**, and S5 for **3**.

Table S1. Crystallographic data for **1**, **2**, and **3**.

compounds	**1**	**2**	**3**
formula	$C_{40}H_{54}CuN_{10}O_3S_2$	$C_{24}H_{32}CuN_6O_2S_2$	$C_{78}H_{88}Cu_3N_{22}S_6$
Fw	850.6	564.22	1716.70
Lattice	*monoclinic*	*triclinic*	*monoclinic*
a, Å	13.688(8)	8.933(7)	33.693(3)
b, Å	13.190(7)	9.721(8)	15.1759(16)
c, Å	23.337(13)	9.751(9)	15.8193(14)
α, °		98.566(8)	
β, °	96.326(9)	102.233(14)	92.281(4)
γ, °		93.892(14)	
V, Å^3	4187(4)	813.9(12)	8082.2(13)
space group	$P2_1/n$ (No. 14)	*P*-1 (No. 2)	*C*2/c (No. 15)
Z	4	1	4
ρ (calcd), g cm^{-3}	1.349	1.151	1.411
μ (MoKα), mm^{-1}	0.672	0.826	0.996
radiation (λ, Å)	0.7107	0.7107	0.7107
temp, *K*	173	293	173
reflns collected	24546	5176	30371
unique reflns	7106	2764	7824
param refined	550	235	502
R_1 [$I > 2\sigma(I)$]	0.0873	0.0729	0.0687
wR_2 [all data]	0.1715	0.1636	0.1271
GOF	1.016	1.011	1.019

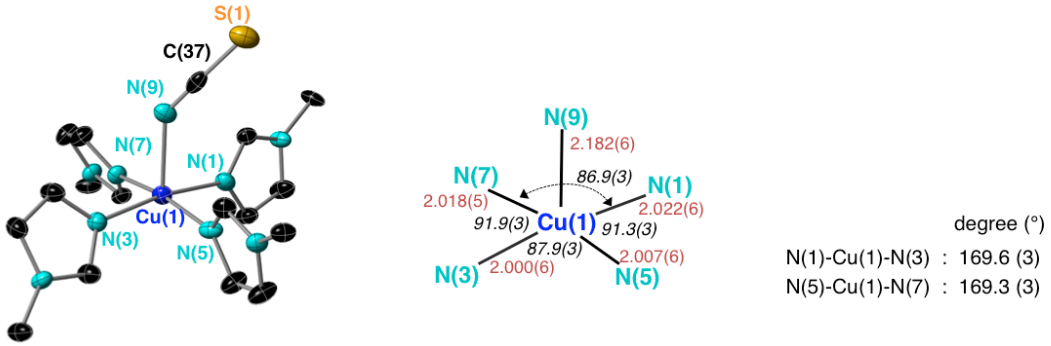

Figure S1. X-ray crystal structure of $\{[Cu(bitb)_2(NCS)]NCS{\cdot}2MeOH{\cdot}H_2O\}_n$ **(1)** represented by thermal ellipsoids of 30% probability; coordination environment around the Cu(II) center. Hydrogen atoms and solvent molecules are omitted for clarity. Color code: blue, copper; cyan, nitrogen; black, carbon; yellow, sulfur.

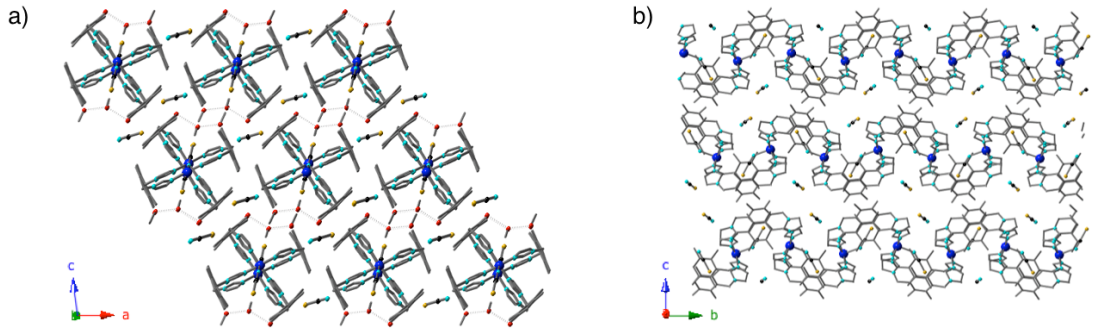

Figure S2. Crystal structures of $\{[Cu(bitb)_2(NCS)]NCS{\cdot}2MeOH{\cdot}H_2O\}_n$ **(1)** viewed down the *b* axis (a) and the *a* axis (b). The alignments of 1D-chains, counter anions, and solvent molecules are shown.

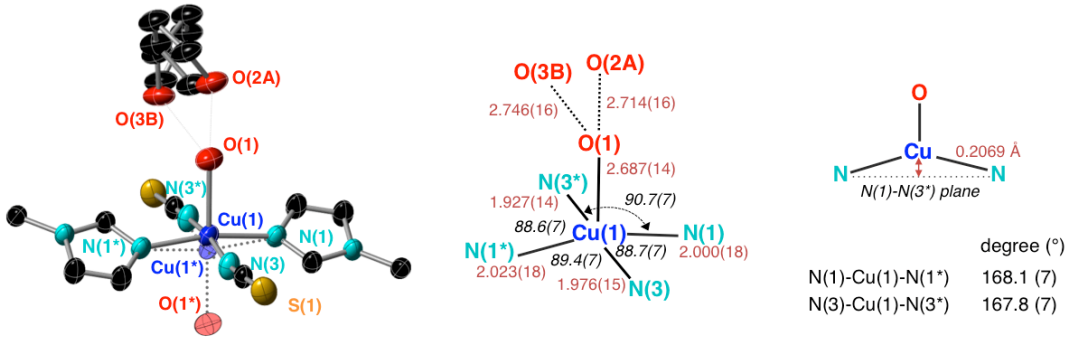

Figure S3. X-ray crystal structure of $\{[Cu(bitb)(NCS)_2(H_2O)]THF\}_n$ **(2)** represented by thermal ellipsoids of 30% probability; coordination environment around the Cu(II) center. Hydrogen atoms are omitted for clarity. Color code: blue, copper; red, oxygen; cyan, nitrogen; black, carbon; yellow, sulfur.

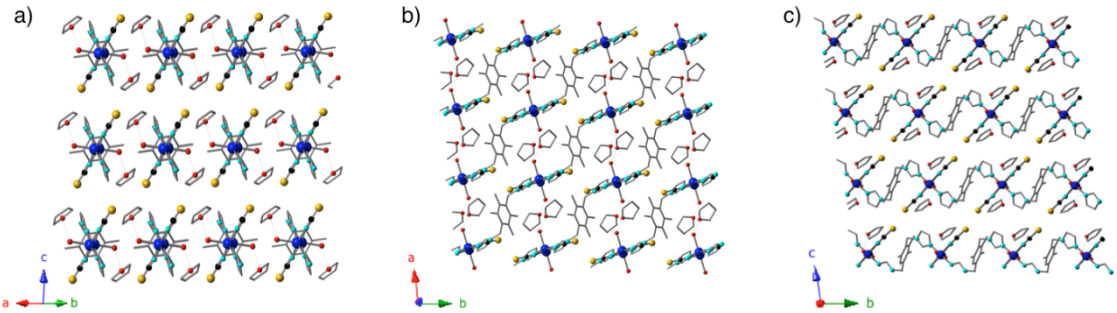

Figure S4.Crystal structures of $\{[Cu(bitb)(NCS)_2(H_2O)]THF\}_n$ **(2)**; the alignments of 1D-chains and solvent molecules along the (*a* +*b*) vector (a),*c* axis (b), and *a* axis (c) are shown.

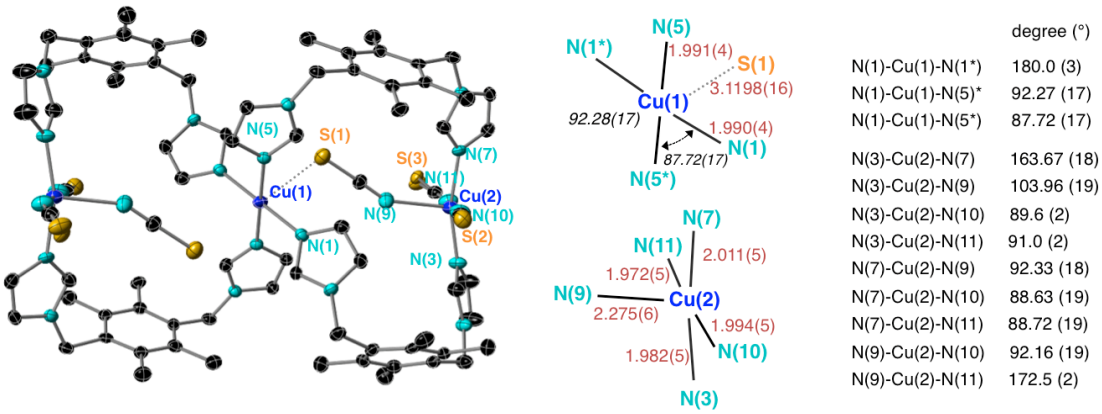

	degree (°)
N(1)-Cu(1)-N(1*)	180.0 (3)
N(1)-Cu(1)-N(5)*	92.27 (17)
N(1)-Cu(1)-N(5*)	87.72 (17)
N(3)-Cu(2)-N(7)	163.67 (18)
N(3)-Cu(2)-N(9)	103.96 (19)
N(3)-Cu(2)-N(10)	89.6 (2)
N(3)-Cu(2)-N(11)	91.0 (2)
N(7)-Cu(2)-N(9)	92.33 (18)
N(7)-Cu(2)-N(10)	88.63 (19)
N(7)-Cu(2)-N(11)	88.72 (19)
N(9)-Cu(2)-N(10)	92.16 (19)
N(9)-Cu(2)-N(11)	172.5 (2)

Figure S5. X-ray crystal structure of $[Cu_3(bitb)_4(NCS)_6]$ **(3)** represented by thermal ellipsoids of 30% probability; coordination environment around the Cu(II) centers and twin-cage structure. Hydrogen atoms and solvent molecules are omitted for clarity. Color code: blue, copper; cyan, nitrogen; black, carbon; yellow, sulfur.

4. X-ray Powder Diffraction (XRPD) Patterns

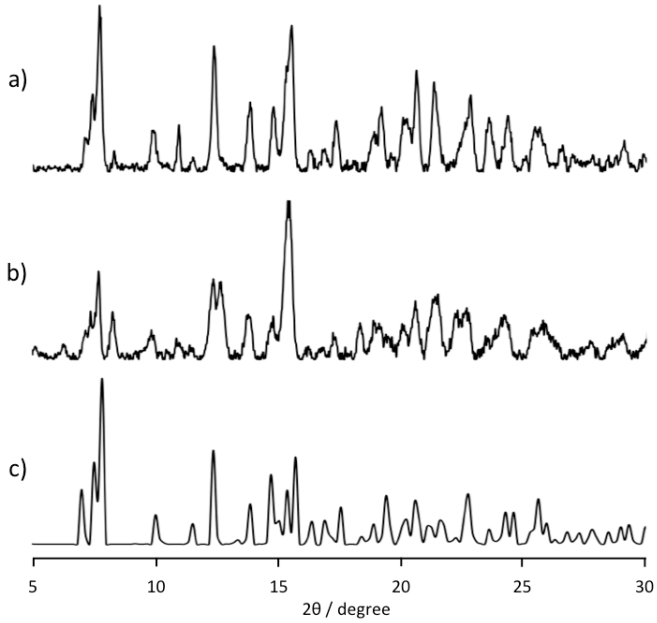

Figure S6. Observed XRPD patterns of blue crystals (a) and bule bulk sample (b) of **1**, and the simulated XRPD pattern based on the single crystal X-ray structure of **1** (c).

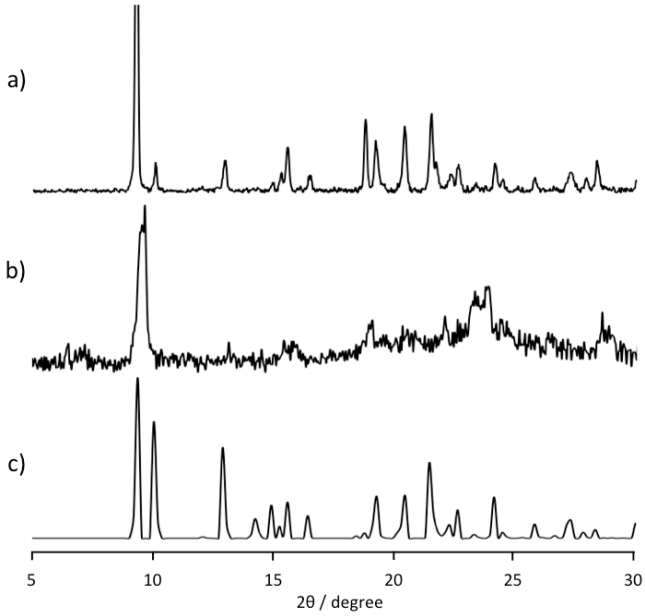

Figure S7. Observed XRPD patterns of green crystals (a) and light green bulk sample (b) of **2**, and the simulated XRPD pattern based on the single crystal X-ray structure of **2** (c).

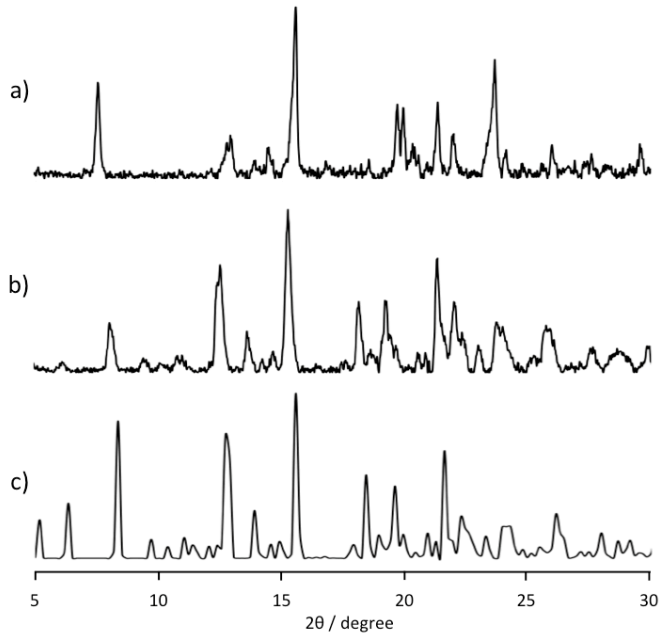

Figure S8. Observed XRPD patterns of green crystals (a) and green bulk sample (b) of **3**, and the simulated XRPD pattern based on the single crystal X-ray structure of **3** (c).

5. XRPD patterns of 1, 2, and 3 before and after contact with organic solvent for study of structural conversions among 1, 2, and 3.

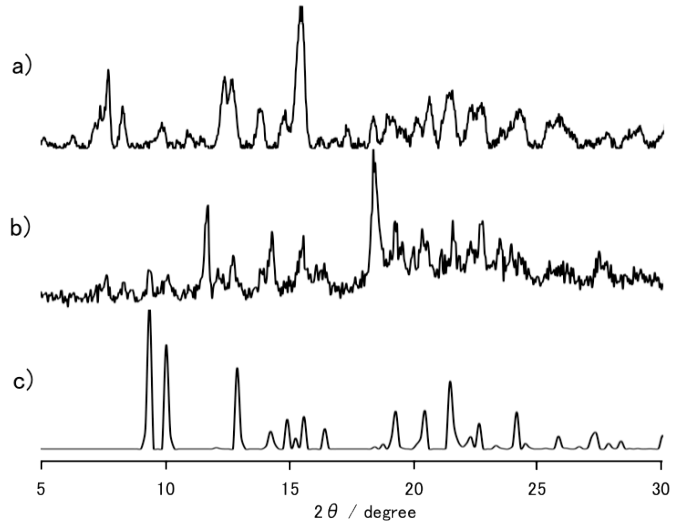

Figure S9. Observed XRPD patterns of flesh powder of **1** (a) and the powder sample obtained after stirring of the bulk sample of **1** in THF for 2 weeks (b), and the simulated XRPD pattern based on single crystal X-ray structure of **2** (c). The XRPD pattern of (b) is not consistent with the simulated pattern of **2** (c), indicating that **1** is not converted to **2** by treatment with THF.

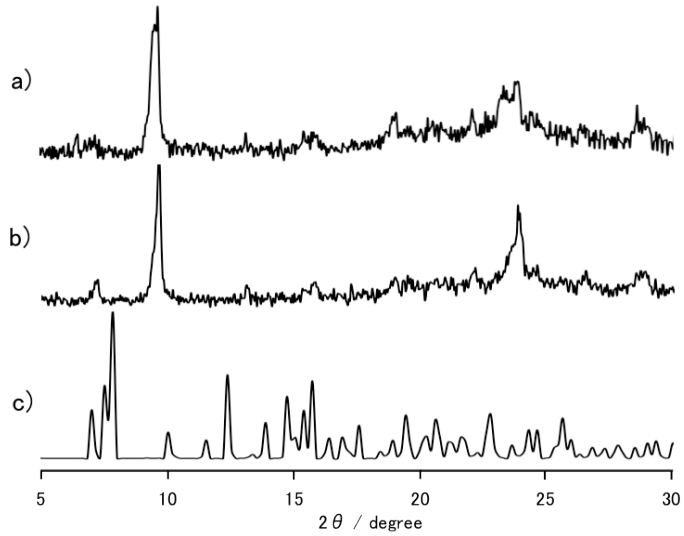

Figure S10. Observed XRPD patterns of flesh powder of **2** (a) and the powder sample obtained after stirring of the bulk sample of **2** in MeOH for 2 weeks (b), and the simulated XRPD pattern based on single crystal X-ray structure of **1** (c). The XRPD pattern of (b) is not consistent with the simulated pattern of **1** (c), indicating that **2** is not converted to **1** by treatment with MeOH.

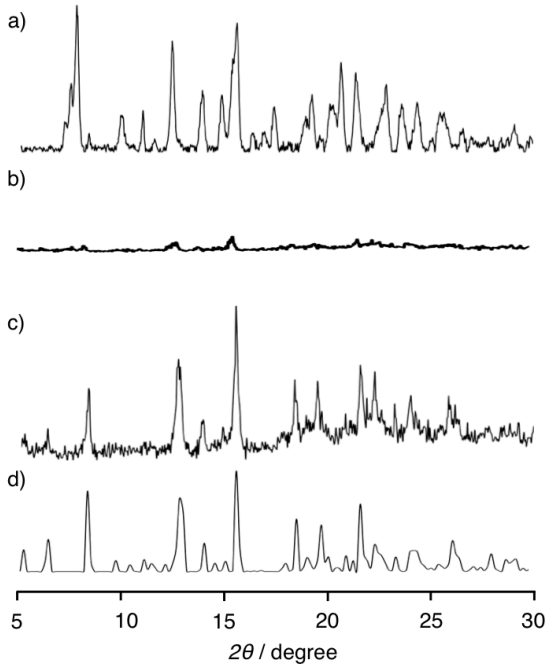

Figure S11. Observed XRPD patterns of flesh powder of **1** (a) and the powder sample obtained after stirring of the bulk sample of **1** in MeCN for 4 days (b) and a week (c), and the simulated XRPD pattern based on single crystal X-ray structure of **3** (d). The XRPD pattern of (c) is consistent with the simulated pattern of **3** (d), indicating that **1** is converted to **3** by treatment with MeCN.

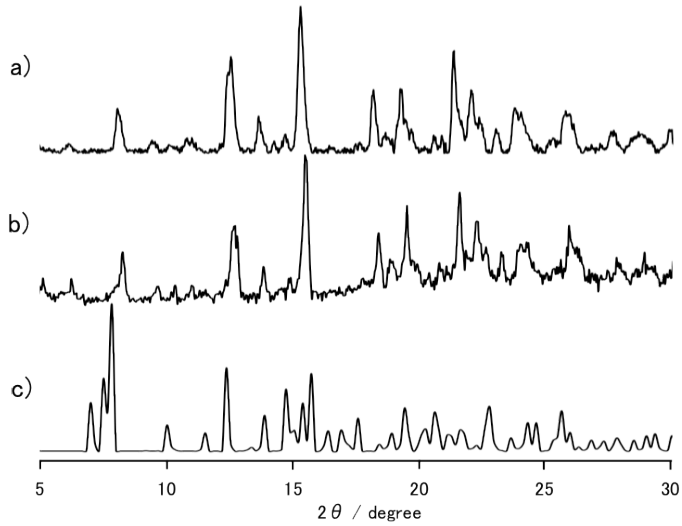

Figure S12. Observed XRPD patterns of flesh powder of **3** (a) and the powder sample obtained after stirring of the bulk sample of **3** in MeOH for 2 weeks, and the simulated XRPD pattern based on single crystal X-ray structure of **1** (c). The XRPD pattern of (b) is not consistent with the simulated pattern of **1** (c), indicating that **3** is not converted to **1** by treatment with MeOH.

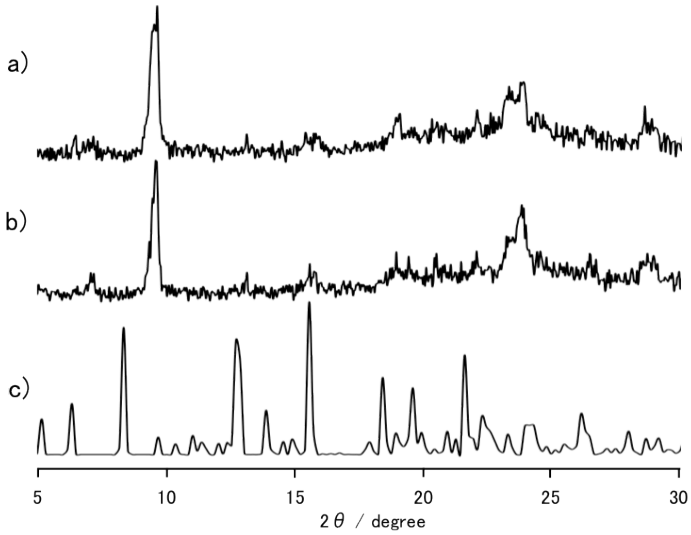

Figure S13. Observed XRPD pattern of flesh powder of **2** (a) and the powder sample obtained after stirring of the bulk sample of **2** in MeCN for 2 weeks, and the simulated XRPD pattern based on single crystal X-ray structure of **3** (c). The XRPD pattern of (b) is not consistent with the simulated pattern of **3** (c), indicating that **2** is not converted to **3** by treatment with MeCN.

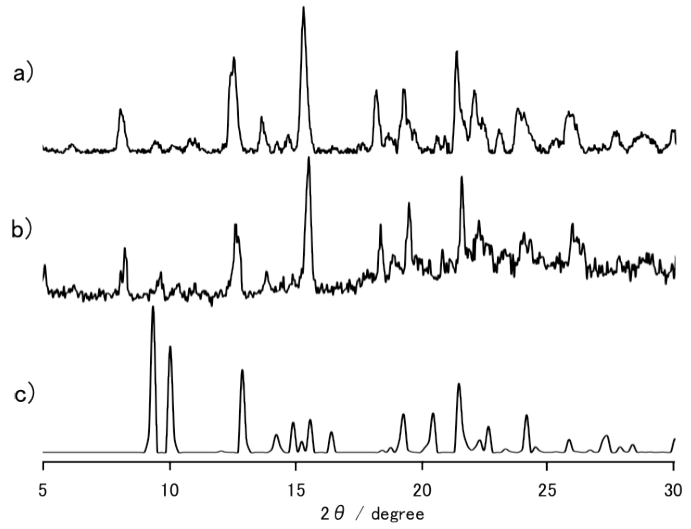

Figure S14. Observed XRPD pattern of flesh powder of **3** (a) and the powder sample obtained after stirring of the sample of **3** in THF for 2 weeks (b) and the simulated XRPD pattern based on single crystal X-ray structure of **2** (c). The XRPD pattern of (b) is not consistent with the simulated pattern of **2** (c), indicating that **3** is not converted to **2** by treatment with THF.

6. IR Spectra Charts

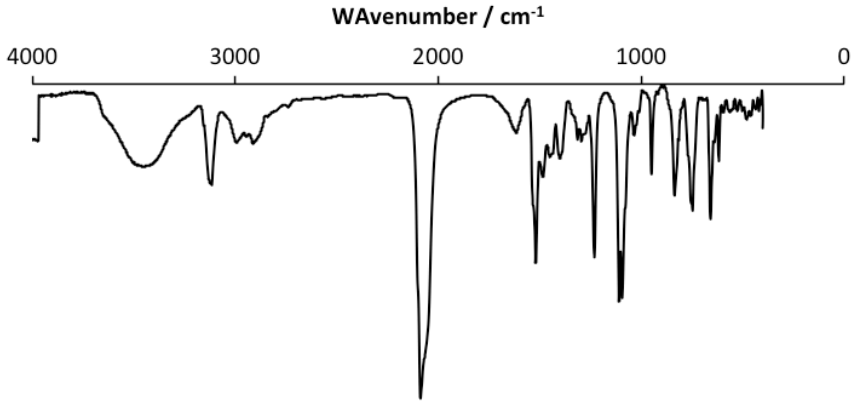

Figure S15. IR spectrum chart of **1.**

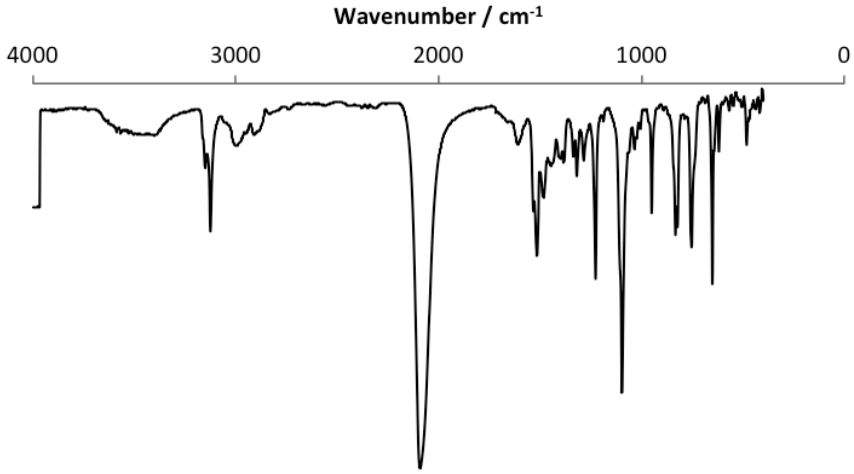

Figure S16. IR spectrum chart of **2**.

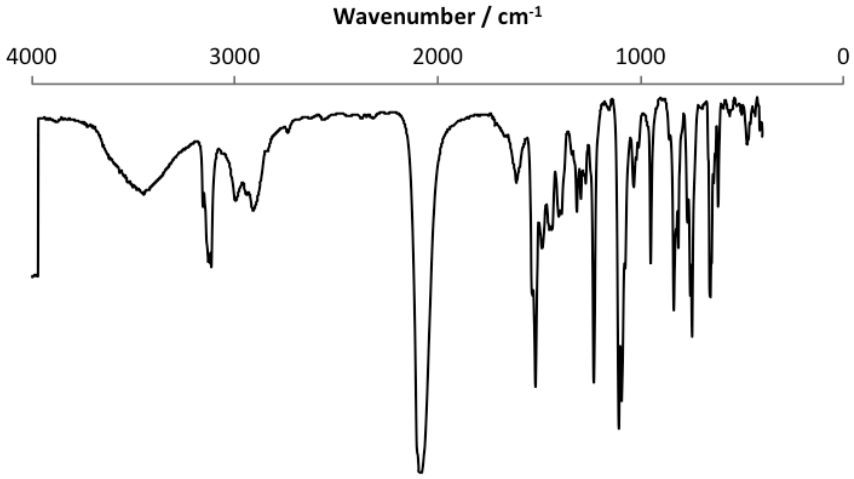

Figure S17. IR spectrum chart of **3**.

7. UV-vis. Reflectance Spectra charts

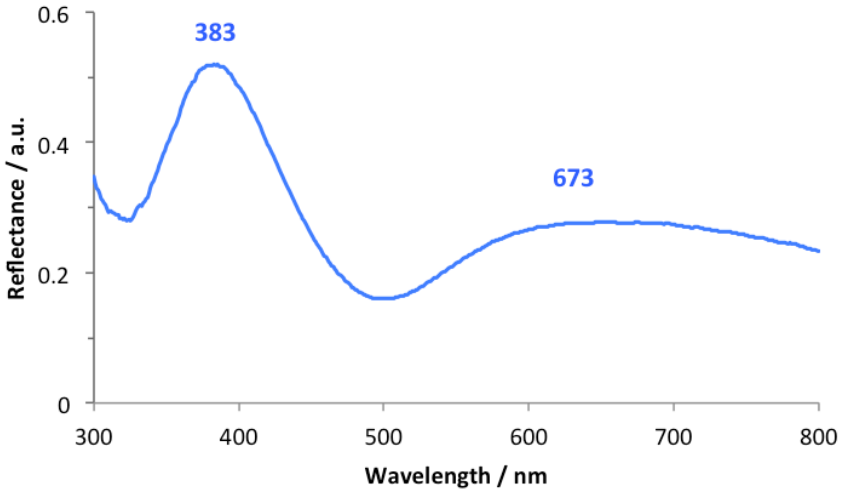

Figure S18. UV-vis. reflectance spectrum chart of **1**.

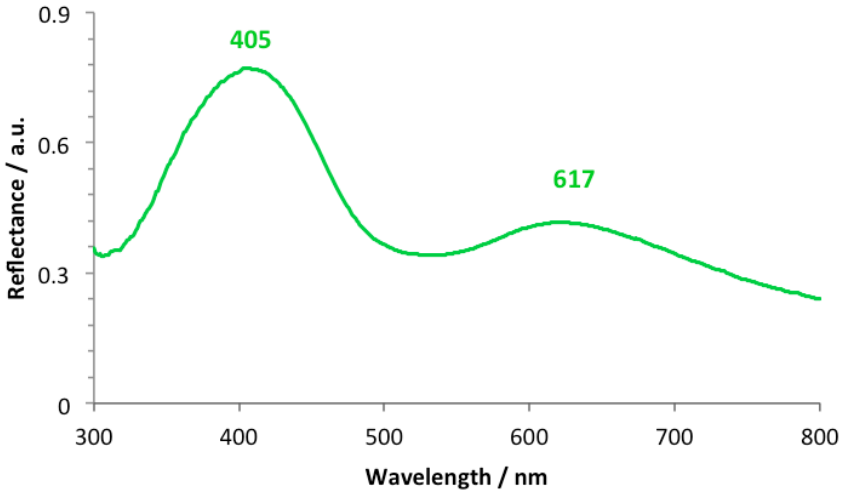

Figure S19. UV-vis. reflectance spectrum chart of **2**.

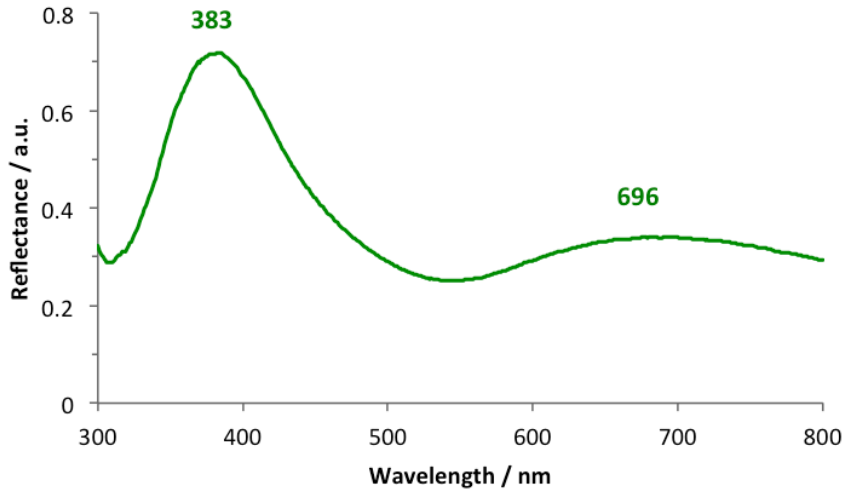

Figure S20. UV-vis. reflectance spectrum of **3**.

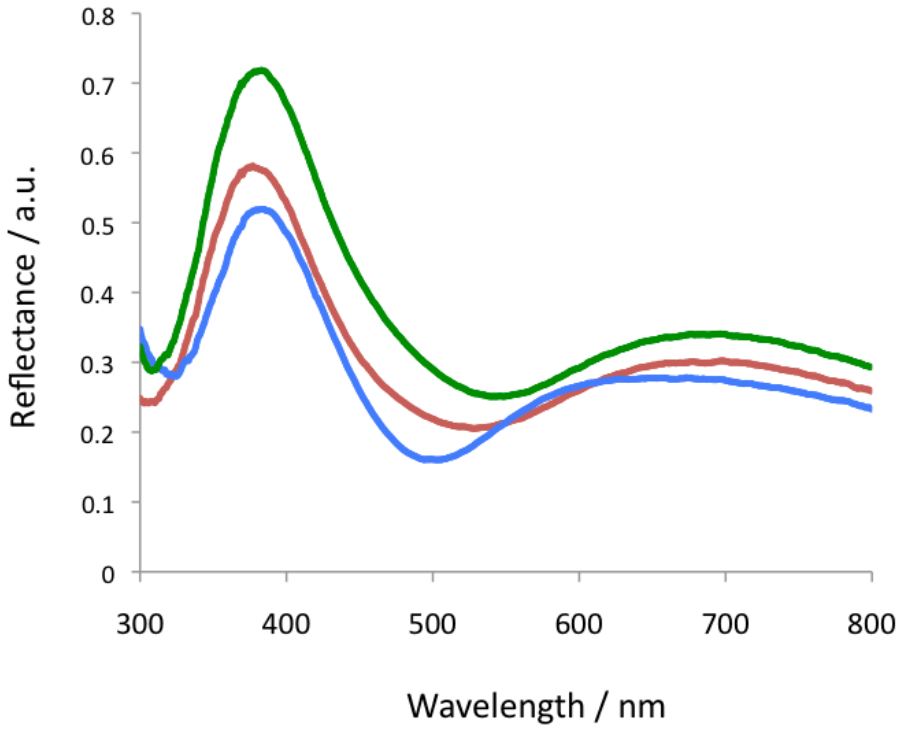

Figure S21. UV-vis. reflectance spectrum of **1** (blue), and the powder sample obtained after stirring of the bulk sample of **1** in MeCN for a week (red), and **3** (green).